Diagn Interv Radiol 2016; 22:141–150

BREAST IMAGING

ORIGINAL ARTICLE

MRI in the differential diagnosis of primary architectural distortion detected by mammography

Lifang Si
Renyou Zhai
Xiaojuan Liu
Kaiyan Yang
Li Wang
Tao Jiang

PURPOSE
We aimed to evaluate the diagnostic accuracy of a combination of dynamic contrast-enhanced magnetic resonance imaging (DCE-MRI) and apparent diffusion coefficient (ADC) values in lesions that manifest with architectural distortion (AD) on mammography.

METHODS
All full-field digital mammography (FFDM) images obtained between August 2010 and January 2013 were reviewed retrospectively, and 57 lesions showing AD were included in the study. Two independent radiologists reviewed all mammograms and MRI data and recorded lesion characteristics according to the BI-RADS lexicon. The gold standard was histopathologic results from biopsies or surgical excisions and results of the two-year follow-up. Receiver operating characteristic curve analysis was carried out to define the most effective threshold ADC value to differentiate malignant from benign breast lesions. We investigated the sensitivity and specificity of FFDM, DCE-MRI, FFDM+DCE-MRI, and DCE-MRI+ADC.

RESULTS
Of the 57 lesions analyzed, 28 were malignant and 29 were benign. The most effective threshold for the normalized ADC (nADC) was 0.61 with 93.1% sensitivity and 75.0% specificity. The sensitivity and specificity of DCE-MRI combined with nADC was 92.9% and 79.3%, respectively. DCE-MRI combined with nADC showed the highest specificity and equal sensitivity compared with other modalities, independent of the presentation of calcification.

CONCLUSION
DCE-MRI combined with nADC values was more reliable than mammography in differentiating the nature of disease manifesting as primary AD on mammography.

Architectural distortion (AD) has been described by the American College of Radiology in its Breast Imaging Reporting and Data System (BI-RADS) as follows: "the normal architecture is distorted with no definite mass visible. This includes spiculations radiating from a point and focal retraction or distortion of the edge of the parenchyma" (1). AD is the third most common mammographic manifestation of nonpalpable breast cancer (2). Primary AD, including all causes without a known history of breast intervention, trauma, or infection, has been found to be associated with breast malignancy in one-half to two-thirds of the cases in which it was observed (3, 4).

Nonetheless, AD may mimic the normal appearance of overlapping breast tissue, which can be subtle and particularly difficult to detect by mammography. Recent studies revealed that AD is the most commonly missed abnormality in false-negative mammography (5). Baker et al. (6) reported that fewer than one-half of cases with AD were detected by the two most widely available computer-aided detection (CAD) systems. Also, AD lesions are associated with diagnostic and management difficulties, given that a board spectrum of benign processes, such as radial sclerosis and sclerosing adenosis, manifest as AD. Furthermore, AD does not always exhibit ultrasound features (3, 7), which increases the difficulty of subsequent biopsy verification. As clinical use of digital breast tomosynthesis (DBT) increases, the addition of DBT to standard two-view mammography can significantly improve the accuracy and false-positive recall rate compared with those of mammography alone (8, 9), especially for dense breast and AD lesions

From the Department of Radiology (R.Z. ✉ *ryzhai219@hotmail.com*), Beijing Chao-Yang Hospital, Capital Medical University, Beijing, China.

Received 15 January 2015; revision requested 24 March 2015; last revision received 29 August 2015; accepted 1 September 2015.

Published online 19 February 2016.
DOI 10.5152/dir.2016.15017

(10). However, DBT requires radiation and cannot be used to evaluate the kinetics of suspicious lesions. Also, a recent publication indicated that DBT is ineffective for differentiating malignant from benign lesions and accurately evaluating the extension of lesions (11). Therefore, a modality that precisely evaluates the nature of AD is critical and needed.

Dynamic contrast-enhanced magnetic resonance imaging (DCE-MRI) has proven to be the most sensitive method for detecting breast cancer (12, 13); however, controversy remains regarding the specificity of this modality, given that previous publications reported a wide range of specificities from 21% to 100% (14–16). One possible solution to improve this is to use apparent diffusion coefficient (ADC) values derived from diffusion-weighted imaging (DWI) to characterize breast tumors, and promising results have been reported by studies that combined ADC values and DCE-MRI in data analysis (17–22). Nevertheless, few investigations have specifically evaluated MRI findings of AD detected by mammography, and moreover, the standard MRI scanning techniques have evolved since publication of these studies (23, 24). Therefore, we aimed to evaluate the diagnostic accuracy of the current standard MRI combined with DWI in the characterization of lesions that manifest with AD on mammography.

Main points

- Architectural distortion (AD) is the third most common mammographic manifestation of nonpalpable breast cancer. Primary AD, including all causes without a known history of breast intervention, trauma, or infection, has been found to be associated with breast malignancy in one-half to two-thirds of the cases in which it was observed.
- Primary AD is subtle and particularly difficult to detect by mammography. Furthermore, AD does not always exhibit ultrasound features, which increases the difficulty of subsequent biopsy verification.
- We found that normalized ADC (nADC) (AUC=0.819) is more accurate than absolute ADC (AUC=0.749) for revealing malignancy, based on the higher AUC value of the former.
- DCE-MRI combined with nADC values was more reliable than mammography in evaluating the nature of disease manifesting as primary AD in mammography.

Methods

Subjects

A retrospective review of records in the medical database was performed for 396 consecutive women who underwent full-field digital mammography (FFDM) and subsequent breast MRI examinations for various indications, including preoperative staging, equivocal mammographic findings, palpable breast mass but equivocal mammography and sonography, and nipple discharge, at our hospital between August 2010 and January 2013. After investigating all FFDM and MRI data, 57 lesions showing AD in 56 patients with complete pathologic results or two-year follow-up data were included in this analysis. The institutional ethics review committee approved this study, and written informed consent from enrolled patients was waived due to the retrospective nature of this study.

MRI was always carried out before obtaining histopathologic results. All patients underwent MRI and FFDM within 14 days. None of the observed breast tissue was surgically altered before MRI examination.

Malignant lesions were confirmed by histopathology results from biopsies or surgical excisions, and benign lesions were confirmed by pathology results or two-year follow-up observation. BI-RADS categories 1–3 were considered negative, and BI-RADS categories 4–5 were considered positive for the analysis.

FFDM examination

Standard craniocaudal (CC) and mediolateral oblique (MLO) viewing of the breasts with full-field digital mammography (FFDM, Senographe DS GE Healthcare) is routinely performed at our institution.

MRI technique

MRI was performed using a 3.0 Tesla scanner (TimTrio, Siemens) with a four-channel bilateral breast surface coil. Patients were imaged in prone position. The MRI protocol is shown in Table 1 according to the acquisition order. ADC maps were created automatically by the MRI system software from the DWI images. During the DCE-MRI image acquisition, 0.1 mmol/kg bodyweight of gadopentetate dimeglumine (Gd-DTPA, Magnevist, Bayer Healthcare) was injected intravenously at a rate of 3 mL/s by an automatic injector, followed immediately by a 20 mL saline solution flush.

Image interpretation

All FFDM and MRI data were reviewed by the same two blinded radiologists who have six and 12 years experience in breast imaging. The readers first evaluated FFDM images without patient identification and corresponding MRI scans, and then assessed MRI scans without referencing FFDM

Table 1. Parameters of MRI sequences on the axial plane

Parameter	T2W turbo IR	Precontrast T1W 3D FLASH	DWI	DCE-MRI	Postcontrast T1W 3D FLASH
Echo time/repetition time (ms)	61/5000	3.29/7.9	80/8300	2.45/5.3	3.78/8
Inversion time (ms)	230	N/A	220	N/A	N/A
b value (s/mm^2)	N/A	N/A	0/800	N/A	N/A
Flip angles (degrees)	80	25	N/A	24.5	12
Number of slices	30	160	24	160	208
Slice gap (mm)	0.8	-	2	-	-
Field of view (cm)	34×34	34×34	34×15	34×34	34×34
Matrix size	320×313	384×284	192×192	448×318	448×407
Bandwidth (Hz)	319	380	1446	350	450
GRAPPA factor	2	2	2	N/A	2
Slice thickness (mm)	4	0.9	4	0.9	0.8
Acquisition time	4 min 12 s	1 min 17 s	2 min 5 s	9 min 49 s	3 min 43 s

T2W, T2-weighted; IR, inversion recovery; T1W, T1-weighted; 3D, three-dimensional; FLASH, fast low angle shot; DWI, diffusion-weighted image; DCE-MRI, dynamic contrast-enhanced magnetic resonance N/A, not available; GRAPPA, generalized autocalibrating partial parallel acquisition.

Table 2. Classification scheme

		Lesion characteristics				
Lesion type	BI-RADS category	Shape	Margin	Internal enhancement	Kinetic curve	nADC value
No enhancement	BI-RADS 1	-	-	-	-	-
Mass						
	BI-RADS 2	Oval lobulated round	Circumscribed	Dark internal septations	Regardless of kinetic curve	Regardless of nADC value
		Oval lobulated round	Circumscribed	Heterogeneous/homogeneous	Persistent	>0.61
	BI-RADS 3	Oval lobulated round	Circumscribed	Heterogeneous/homogeneous	Persistent	<0.61
		Oval lobulated round	Circumscribed	Heterogeneous/homogeneous	Plateau/washout	>0.61
	BI-RADS 4	Oval lobulated round	Circumscribed	Heterogeneous/homogeneous	Plateau/washout	<0.61
		Irregular	Not circumscribed	Rim enhancement/ heterogeneous/homogeneous	Persistent/plateau	>0.61
	BI-RADS 5	Irregular	Not circumscribed	Rim enhancement/ heterogeneous/homogeneous	Persistent/plateau	<0.61
		Irregular	Not circumscribed	Rim enhancement/ heterogeneous/homogeneous	Washout	Regardless of nADC value
NME						
	BI-RADS 2	Focal	-	Homogeneous	Persistent/plateau	Regardless of nADC value
	BI-RADS 3	Focal	-	Heterogeneous	Persistent/plateau	Regardless of nADC value
		Focal	-	Homogeneous	Washout	Regardless of nADC value
		Regional	-	Homogeneous	Persistent	>0.61
	BI-RADS 4	Regional	-	Homogeneous	Persistent	<0.61
		Segmental/ductal/linear	-	Regardless of internal enhancement	Regardless of kinetic curve	>0.61
	BI-RADS 5	Segmental/ductal/ linear/regional		Clumped/clustered ring/ heterogeneous	Regardless of kinetic curve	<0.61

BI-RADS, breast imaging reporting and data system; nADC, normalized apparent diffusion coefficient; NME, non-mass enhancement.

images. After the evaluation was done, both radiologists had access to all imaging data, and controversial findings were discussed by the two radiologists until consensus was reached. BI-RADS was used as the reference standard for AD (1).

The AD lesions detected by FFDM were categorized as lesions with or without calcification(s). Readers described the breast tissue density, lesion location, shape of calcifications, and other associated findings (skin retraction, nipple retraction, and axillary adenopathy). According to their shapes, calcifications were classified as coarse heterogeneous, amorphous, fine pleomorphic, fine linear, or punctate. A BI-RADS category was assigned by the readers.

The MRI findings were reviewed in three steps. In the first step, readers had access only to the DCE-MRI data. They were blinded to the current clinical evaluation and FFDM findings, whereas the data for patients' personal history of breast cancer and prior MRI were available. If an enhanced lesion was discovered, the location, lesion type, shape, border, distribution, kinetics, and internal architecture were carefully recorded according to the BI-RADS lexicon. Based on the above findings, the final MRI assessment was performed according to BI-RADS for MRI. The classification scheme is summarized in Table 2. The second step included analysis of FFDM images, and this information was subsequently correlated with DCE-MRI results to obtain a new general BI-RADS classification (BI-RADS DCE-MRI+FFDM) using a five-point scale (1, negative; 2, benign finding; 3, probable benign finding; 4, suspicious abnormality; 5, highly suggestive of malignancy) according to the following principle: if FFDM revealed fine pleomorphic or fine linear calcifications, the case was classified as BI-RADS 5, regardless of the manifestation on DCE-MRI; the other AD lesions were classified into different BI-RADS categories based on DCE-MRI manifestation. Finally, DWI findings and ADC maps were evaluated. The mean absolute ADC for the suspicious lesion of interest (ADC_{int}) and the glandular tissue (ADC_{ref}) were calculated. The normalized ADC (nADC) was then calculated using the following formula: $nADC=ADC_{int}/ADC_{ref}$. DCE-MRI combined with nADC values was also used to obtain a new BI-RADS classification (BI-RADS DCE-MRI+ADC) using the same five-point scale indicated for the second step.

For each lesion detected on DCE-MRI, a region of interest (ROI) was defined at the corresponding location on the ADC images. The ROI was drawn freehand to include the area of hypointensity to encompass as

much of the abnormality as possible. ROIs for evaluation of normal fibroglandular tissue were placed on the contralateral breast at areas where no suspicious lesions were reported. During the ROI placement, care was taken to avoid regions with high T2 signal within a lesion, such as a cyst, hematoma, or necrosis, by verifying the ROI against the T2-weighted image. In case a lesion was not hyperintense on DWI, the ROI was drawn at the corresponding location on a DCE-MRI image presenting a suspicious lesion.

Statistical analysis

Receiver operating characteristic (ROC) curve analysis was carried out to determine the threshold ADC value to differentiate malignant from benign breast lesions. We determined the best cutoff value using Youden statistics, Y=sensitivity-(1-specificity), which allows a balance between high sensitivity and specificity. The sensitivity, specificity, positive predictive value (PPV), and negative predictive value (NPV) of FFDM, DCE-MRI, FFDM+DCE-MRI, and DCE-MRI+ADC were calculated based on a gold standard of pathologic or follow-up results. We calculated 95% confidence intervals (CIs) from the normally approximated binomial distribution. We compared the ADC values and nADC values of two groups using the Mann-Whitney U test and analyzed categorical data using Fisher exact test and Fisher-Freeman-Halton test. $P < 0.05$ was considered statistically significant. All statistical analyses were performed using SPSS 17.0 (SPSS Inc.) and MedCalc 10.5.4 (MedCalc Software).

We analyzed false-positive and false-negative cases to clarify the limitations of using MRI for differential diagnosis.

Results

A total of 57 lesions from 56 patients (age range, 27–78 years; median age, 48 years) were analyzed. Forty-five lesions were verified by surgical pathology findings and/or percutaneous biopsy, and the remaining 12 benign lesions were verified by follow-up for ≥2 years, during which no malignancy was observed at the location of primary suspicion.

Histologic diagnoses included 28 malignant (17 invasive ductal carcinomas, seven ductal carcinoma in situ, one invasive lobular carcinoma, two mucinous carcinoma, one apocrine carcinoma) and 17 benign lesions (one plasma cell mastitis, three fibrocystic diseases, one fibroadenomas, four intraductual papillomas, three atypical ductal epithelial hyperplasia, and five sclerosing adenosis).

Table 3. Sensitivity and specificity of different modalities and ADC values in AD with or without calcifications

	Modalities	AD with calcification	*P*	AD without calcification	*P*
SE (%)	FFDM	87.5	1.000	66.6	0.0932
	DCE-MRI+ADC	87.5		100	
	DCE-MRI	87.5		91.7	
	FFDM+DCE-MRI	87.5		100	
SP (%)	FFDM	17.6	0.008	0	0.003
	DCE-MRI+ADC	70.6		91.7	
	DCE-MRI	47.1		33.3	
	FFDM+DCE-MRI	47.1		33.3	
ADC_{int} ($\times 10^{-3}$ mm^2/s)	Benign	1.29	0.011	1.44	0.026
	Malignant	1.14		1.01	
nADC	Benign	0.805	0.002	0.878	0.002
	Malignant	0.622		0.549	

ADC, apparent diffusion coefficient; AD, architectural distortion; SE, sensitivity; FFDM, full-field digital mammography; DCE-MRI, dynamic contrast-enhanced magnetic resonance imaging; SP, specificity; ADC_{int}, absolute ADC; nADC, normalized ADC.

The ADC_{int} values of malignant and benign lesions were 1.08×10^{-3} mm^2/s and 1.35×10^{-3} mm^2/s, respectively ($P = 0.001$). The nADC values of malignant and benign lesions were 0.588 and 0.832, respectively ($P < 0.001$). The ADC_{int} values and nADC values of AD with and without calcification are shown in Table 3. The ADC_{int} values and nADC values of malignant lesions were lower than those of the benign lesions, and the differences were statistically significant independent of the presence of calcification ($P = 0.011$ and $P = 0.002$ with calcification, respectively, and $P = 0.026$ and $P = 0.002$ without calcification, respectively).

The ROC curves of the ADC values are shown in Fig. 1. When the threshold of ADC_{int} was set at 1.19×10^{-3} mm^2/s, the sensitivity and specificity were 72.4% and 85.7%, respectively. For a nADC value threshold of 0.61, the sensitivity and specificity were 93.1% and 75.0%, respectively. The area under the curve (AUC) for nADC was higher than that for ADC_{int} (0.819 vs. 0.749, respectively, $P = 0.011$).

An example of the typical presentation of AD on mammography and DCE-MRI and the corresponding pathologic findings are shown in Fig. 2. Table 4 reveals the association between the individual modalities and their histopathology/follow-up results, and shows the corresponding sensitivity, specificity, PPV, and NPV values of each modality. The sensitivity of DCE-MRI was higher than that of FFDM (89.3% vs. 78.6%), but this difference was not significant ($P = 0.510$). The specificity of DCE-MRI alone was significantly higher than that of FFDM ($P = 0.039$). DCE-MRI+ADC provided even higher specificity compared with DCE-MRI (79.3% vs. 41.4%, respectively; $P = 0.010$), without a significant decrease in the sensitivity. The sensitivity of FFDM+DCE-MRI was higher than that of DCE-MRI, but the difference was not significant (92.9% vs. 89.3%, $P = 1.000$). The specificities of the two methods were equal (41.4%). No statistically significant difference was observed between the performances of DCE-MRI and FFDM+DCE-MRI.

Table 3 shows the diagnostic sensitivities and specificities for AD with and without calcification. There was a statistically significant difference between the specificity of FFDM and that of DCE-MRI+ADC ($P = 0.003$) in detecting underlying disease showing AD without calcification, and the same difference was revealed between DCE-MRI and DCE-MRI+ADC ($P = 0.023$). Similarly, a significant difference was observed between the specificity of FFDM and that of

Table 4. The diagnostic results of the four modalities and the association between BI-RADS categories and final results

Modality	BI-RADS categories	Benign lesions[a]	Malignant lesions[b]	SE (95% CI)	SP (95% CI)	PPV (95% CI)	NPV (95% CI)
FFDM	3[c]	3	6	78.6 (59.0–91.7)	10.3 (2.3–27.4)	45.8 (31.4–60.8)	33.3 (7.9–70.0)
	4-5	26	22				
DCE-MRI	1-3	12	3	89.3 (71.8–97.6)	41.4 (23.5–61.1)	59.5 (43.3–74.4)	80.0 (51.9–95.4)
	4-5	17	25				
FFDM+DCE-MRI	1-3	12	2	92.9 (76.5–98.9)	41.4 (23.5–61.1)	60.5 (44.4–75.0)	85.7 (57.2–97.8)
	4-5	17	26				
DCE-MRI+ADC	1-3	23	2	92.9 (76.5–98.9)	79.3 (60.3–92.0)	81.3 (63.6–92.8)	92.0 (73.9–98.8)
	4-5	6	26				
Total		29	28	-	-	-	-

[a]Histology/follow-up results; [b]Histology; [c]No finding in BI-RADS categories 1 and 2.
BI-RADS, breast imaging reporting and data systems; SE, sensitivity; SP, specificity; PPV, positive predictive value; NPV, negative predictive value; 95% CI, 95% confidence interval; FFDM, full-field digital mammography; DCE-MRI, dynamic contrast-enhanced magnetic resonance imaging; ADC, apparent diffusion coefficient.

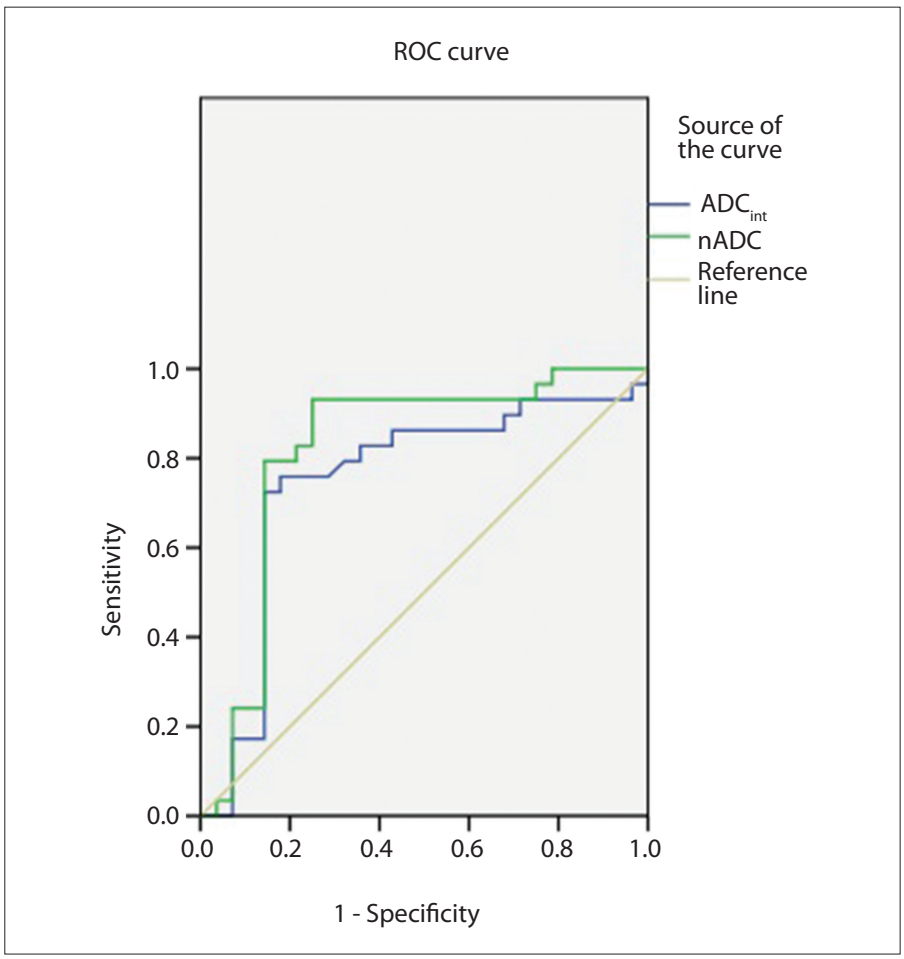

Figure 1. The comparison of ROC curves between absolute (ADC_{int}) and normalized (nADC) apparent diffusion coefficients. Area under the curve of nADC is significantly higher than that of ADC_{int} ($P = 0.011$).

DCE-MRI+ADC in identifying lesions showing AD with calcification ($P = 0.008$). The diagnostic sensitivity of FFDM did not differ significantly for AD with and without calcification ($P = 0.354$). The six false-negative cases included eight lesions without calcification and one lesion with calcification.

Among 11 benign AD lesions with calcification, there were two coarse heterogeneous, two amorphous, one fine pleomorphic, and six punctate calcifications; in 22 malignant AD lesions with calcification, three coarse heterogeneous, two amorphous, nine fine pleomorphic, seven fine linear, and one punctate calcification were observed. Punctate calcification was more commonly seen in benign lesions ($P = 0.003$). As shown in Table 5, AD mainly manifests as mass (22/57, 38.6%) and non-mass enhancement (NME, 26/57, 45.6%), which contributes to the majority of lesion types on MRI ($P = 0.01$). However, no difference was found in the proportion of malignancy between mass-like and NME lesions ($P = 0.600$). In 22 mass lesions, malignancy was more likely to present an irregular shape ($P = 0.030$) and uncircumscribed margin ($P = 0.010$). Of 26 NME lesions, 13 showed segmental distribution and five presented with clustered ring internal enhancement; however, no statistical difference was observed between benign and malignant lesions ($P = 0.120$ and $P = 0.190$, respectively). There were no statistical differences when considering MRI background parenchymal enhancement, mass and NME internal enhancement, and NME distribution in verifying malignancy. A significantly higher percentage of malignant lesions was detected in cases showing high T2 signal intensity ($P = 0.024$) and kinetic curves classified as "washout" ($P = 0.001$).

The six false-positive cases identified upon applying the DCE-MRI+ADC value consisted of one case of plasma cell mastitis (showing NME with regional distribution, clustered ring internal enhancement, washout kinetic curve, ADC_{int}

Table 5. FFDM and DCE-MRI characteristics of 57 lesions in the study

Diagnostic data	Benign (n=29)	Malignant (n=28)	*P*
Premenopausal women	16	13	0.510
Postmenopausal women	13	15	
AD with calcification	11	22	0.002
AD without calcification	18	6	
FFDM breast density			
1	0	0	0.410
2	4	2	
3	17	21	
4	8	5	
MRI background parenchymal enhancement			
Mild	4	2	0.570
Minimal	13	11	
Moderate	7	6	
Marked	5	9	
MRI lesion type			
Focus	4	0	0.007
Mass	8	14	
NME	12	14	
No enhancement	5	0	
Mass shape[a]			
Oval lobulated round	3	0	0.030
Irregular	5	14	
Mass margin[a]			
Circumscribed	4	0	0.010
Not circumscribed	4	14	
Mass internal enhancement[a]			
Homogeneous	2	0	0.110
Heterogeneous	4	11	
Rim enhancement	1	3	
Dark internal septations	1	0	
NME distribution[b]			
Focal	2	0	0.190
Linear/ ductal	1	3	
Segmental	4	9	
Regional	2	1	
Multiple regions	3	1	
NME internal enhancement[b]			
Homogeneous	0	4	0.061
Heterogeneous	8	5	
Clumped	3	1	
Clustered ring	1	4	
High T2 signal intensity	8	16	0.024
Kinetic curve			
Persistent	7	1	0.008
Plateau	9	7	
Washout	8	20	

[a]n=22, MRI lesion type was mass. [b]n=26, MRI lesion type was non-mass enhancement.
FFDM, full-field digital mammography; DCE-MRI, dynamic contrast-enhanced magnetic resonance imaging; AD, architectural distortion; MRI, magnetic resonance imaging; NME, non-mass enhancement.

<1.19×10^{-3} mm^2/s, nADC <0.61, and maximum dimension of 5.2 cm), three cases of sclerosing adenosis (all showing NME, regional/segmental/focal distribution and heterogeneous internal enhancement, ADC_{int} <1.19×10^{-3} mm^2/s, nADC <0.61, and maximum dimensions of 4.1 cm, 3.2 cm, and 1.7 cm, respectively), and one case of intraductual papilloma (showing NME with segmental distribution, clustered ring internal enhancement, washout kinetic curve, ADC_{int} <1.19×10^{-3} mm^2/s, nADC <0.61, and maximum dimension of 3.8 cm), while the two false-negative cases included one case of ductal carcinoma in situ (stippled distribution, not revealed in DWI, and maximum dimension 1.1 cm), and one case of mucinous carcinoma (lobulated shape, circumscribed margin, heterogeneous internal enhancement with high T2-weighted image signal, ADC_{int} >0.19×10^{-3} mm^2/s, nADC >0.61, and maximum dimension of lesion 1.3 cm).

Discussion

In this study, the specificity of DCE-MRI for revealing malignancy related to AD was significantly higher than that of FFDM. In addition, the combination of ADC values improved the specificity of DCE-MRI, independent of the presence of calcification in the lesion.

We found the specificity of FFDM for AD lesions as 10.3%, which is lower than the specificity of 39.7% for breast cancer reported by a previous study (25). Lesions showing AD are challenging to diagnose and remain a common cause of false-negative mammography, because of subtlety and variability in presentation. The six false-negative cases included eight lesions without calcification and one lesion with calcification. The specificity of DCE-MRI for detecting breast cancer is controversial, ranging from 21% to 100%. A previous study by Cilotti et al. (26) showed no statistically significant difference between the specificities of mammography and MRI for the diagnosis of calcified lesions. In our study, the specificity of DCE-MRI alone was higher than that of FFDM alone. Current researches evaluating the potential of DWI for improving breast imaging are promising. Recent single-center studies have shown that ADC measures are complementary to DCE-MRI parameters for differ-

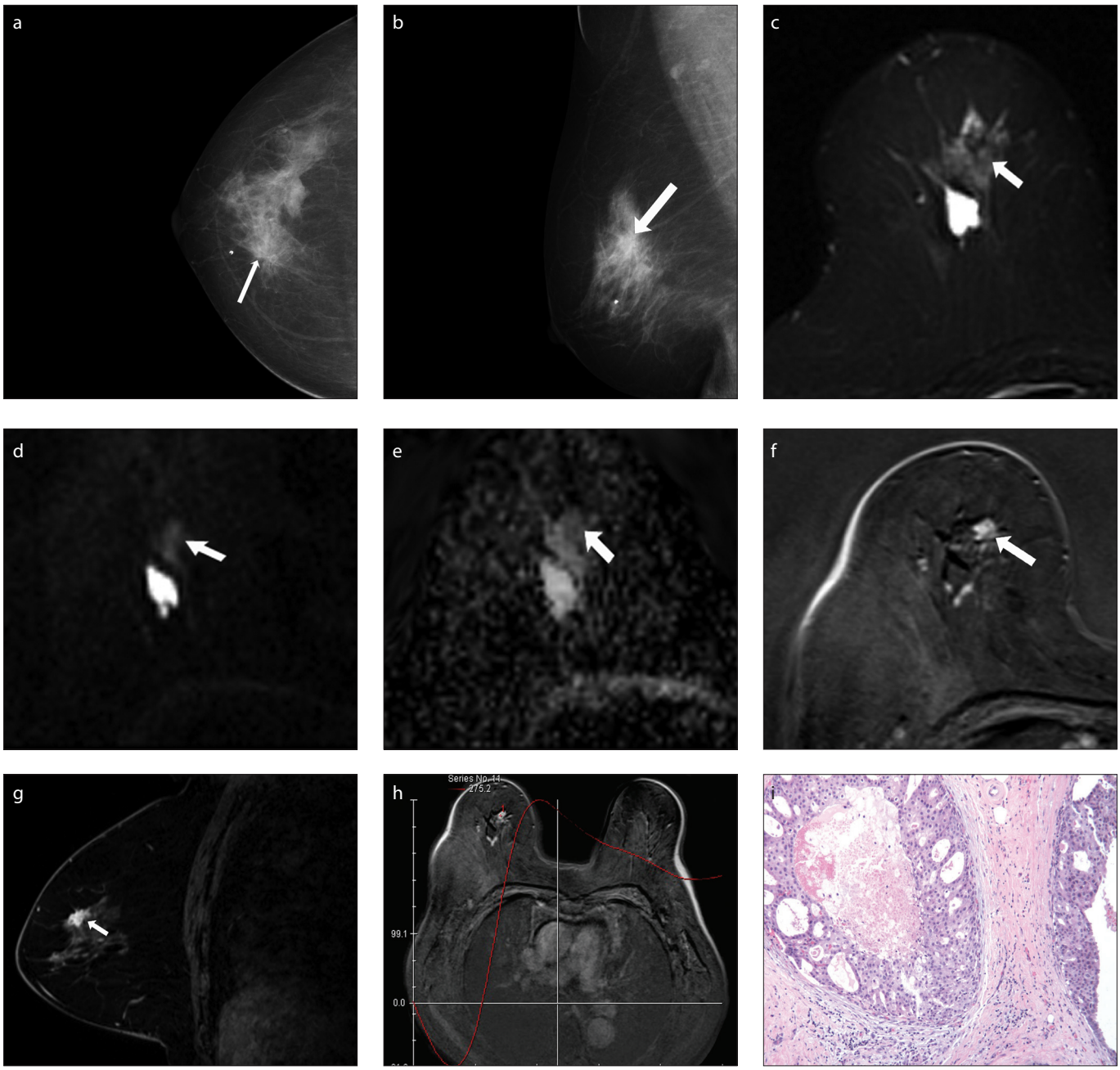

Figure 2. a–i. A 52-year-old female patient presented typical architectural distortion. Mammography craniocaudal **(a)** and mediolateral oblique views **(b)** of the right breast show architectural distortion *(arrows)* in inner upper quadrant. Axial T2-weighted turbo inversion recovery image **(c)** shows an irregular nodule *(arrow)* with low signal. Diffusion-weighted image **(d)** shows slightly high signal *(arrow)*. Apparent diffusion coefficient map **(e)** shows low signal (arrow); the ADC_{int} and nADC values are 1.02×10^{-3} mm^2/s and 0.59, respectively. Axial dynamic contrast-enhanced and subtracted T1-weighted image **(f)** shows irregular nodule with early significant enhancement *(arrow)*. Sagittal postcontrast axial T1-weighted image **(g)** shows an irregular spiculated nodule *(arrow)*. Enhancement kinetic curve **(h)** shows a washout pattern. Pathologic results **(i)** show ductal carcinoma in situ.

entiation of benign and malignant breast lesions and may increase the accuracy of conventional breast MRI assessment (17, 19). Ei Khouli et al. (17) showed that ADC values significantly improved the ability of DCE-MRI to discriminate between benign and malignant lesions. Yabuuchi et al. (21, 22) concluded that the application of DWI together with DCE-MRI contributes to an improved diagnostic accuracy of breast MRI. We found that DCE-MRI combined with ADC values provides a higher specificity than DCE-MRI in AD lesions detected by FFDM, independent of whether calcification is present or absent in the lesion. Thus, with the combination of DCE-MRI and ADC, it might be possible to avoid both unnecessary surgical procedures for benign lesions and missing malignancies presenting as AD. Nevertheless, these possible advantages should be further investigated in a future study with a larger population and longer follow-up.

Our results also showed the preferable sensitivity of DCE-MRI (89.3%) and DCE-MRI combined with ADC (92.9%) compared with that of FFDM (78.6%). However, no statistically significant differences were observed among the sensitivities of the three modalities. The diagnostic sensitivity

of FFDM for AD with calcification appeared to be higher than that for AD without calcification, but the difference was not statistically significant. This could be due to the relatively small sample size. In addition, FFDM is more sensitive for lesions with calcification. In our study, more than 50% of the cases presented with calcification(s) (33/57), and this may also explain our results. Another interesting finding in this study was that the calcification shape showed no difference between benign and malignant lesions except for punctuate calcification, which is not consistent with the findings of a previous study by Uematsu et al. (27). The latter one showed that 25% of amorphous microcalcifications, 64% of pleomorphic microcalcifications, and 92% of linear microcalcifications were malignant. However, it only evaluated screening mammography in detecting pure microcalcification lesions.

We found that nADC (AUC=0.819) is more accurate than ADC_{int} (AUC=0.749) for revealing malignancy, based on the higher AUC value of the former. This result is also consistent with those of previous studies. El Khouli et al. (17) also found that normalized ADCs showed better diagnostic value than absolute ADCs for distinguishing benign lesions from malignant tumors. Prior studies have investigated the role of DWI in breast MRI, and promising results revealed that ADC values have a potential in the differentiation of benign and malignant lesions, providing an absolute ADC threshold value ranging from 1.1×10^{-3} mm^2/s to 1.6×10^{-3} mm^2/s (28–32). Our study revealed an absolute ADC threshold value within this range. However, some overlap remained in the ADCs between benign and malignant lesions, and the degree of overlap was substantially reduced by normalizing the ADC values to those of remote glandular tissue. We observed improvement in the diagnostic model when normalized ADCs were added to conventional MRI data. These results suggest a potential role for nADC values in improving the diagnostic performance of breast MRI for AD lesions detected by FFDM.

In our study, AD detected by FFDM mainly manifested as mass (22/57, 38.6%) and NME (26/57, 45.6%) in DCE-MRI, and no significant differences were observed between benign and malignant lesions. The proportion of malignancy was noticeably higher within masses with an irregular shape and those without a circumscribed margin. The irregular shape and uncircumscribed margins of mass lesions on MRI could be missed in FFDM due to tissue overlap and the simple appearance of AD showing spiculations radiating from a point or focal retraction. However, with the help of MRI, the risk of missed diagnosis can be lowered.

Although DCE-MRI+ADC presented remarkably high sensitivity, there were still false-positive cases in this study. However, all of these cases manifested with NME and an ADC_{int} less than the threshold value. Typical causes of NME include mastopathic changes, fibrocystic changes due to hormonal stimulation, inflammatory changes in benign lesions or ductal carcinoma in situ (DCIS), invasive lobular carcinoma, and some cases of estrogen receptor-negative invasive ductal carcinoma. A previous study reported that NME was the major cause of false-positive breast findings (33). A previous study by Partridge et al. (32) reported that for the same b value, the diagnostic performance of ADC was lower in NME lesions compared with masses larger than 1 cm (34). Another study carried out by the same researchers also suggested that ADC measurements may be more valuable for distinction of masses than for differentiating lesions with NME (35). We also found that there was no statistical difference when considering NME internal enhancement and NME distribution in verifying malignancy. This finding is not consistent with that of a previous study by Tozaki et al. (36) who found that segmental distribution, heterogeneous internal enhancement, and clustered ring enhancement were the most frequent findings in malignant NME. Some specific tumor subtypes, such as papillary carcinoma, are associated with the lowest ADC values among malignant breast tumors (37). On the other hand, their ADC values are very similar to those observed for benign papillomas (38), indicating the histologic similarity between benign and malignant papillary lesions. A diagnostic challenge is also encountered with percutaneous core biopsy and dynamic breast MRI. In addition, sclerosing adenosis can be difficult to distinguish from infiltrating carcinoma. No specific MRI findings have been described for this diagnosis. Usually, ultrasonography does not reveal a focal abnormality, although in minority of cases, a circumscribed mass may be seen with the nodular variant of this condition.

The false-negative cases included one case of DCIS and one case of mucinous carcinoma. In our work, the DCIS case showed focal enhancement and DWI was negative. It is difficult to apply morphologic descriptors in small focal enhancement, and some tiny foci in DCE-MRI could be artifacts. Accordingly, BI-RADS descriptors are currently not applied to assess morphologic and dynamic profiles of foci (39). In addition, previous studies reported that the ability of DWI to detect lesions smaller than 1 cm is limited due the limited ability of ADC maps to depict smaller lesions (27, 38). A later study was able to evaluate all lesions detected with contrast-enhanced MRI, including lesions with a diameter less than 1 cm, which accounted for less than 50% of lesions studied by Partridge et al. (32). In clinical practice, AD in the setting of DCIS is thought to be attributable to a mixture of sclerosing adenosis, sclerosis in the interstitium around the DCIS, and DCIS involving Cooper's ligaments. Prior publications have shown that DCIS with an area of AD occurs in about 7%–13% of the cases (40, 41). In our study, the case of DCIS showed focal enhancement and DWI was negative, even though focal enhancement is usually the least common finding, being seen in only 1%–12% of cases (42, 43). The reported sensitivity of MRI for the detection of DCIS is lower than that for the detection of invasive breast cancers. The case of mucinous carcinoma displayed the highest ADC values, a high signal in T2-weighted imaging, a circumscribed margin, and a persistent enhanced pattern on the kinetic curve in this study. Also, the size of the tumor was small (<1 cm). All the above characteristics led to a misdiagnosis of fibroadenoma.

Some other limitations in our study still require further investigation. First, this was a retrospective study including only a small number of patients. Second, we did not compare the diagnostic performance of ultrasonography, given that more than one-third of the patients' ultrasonography results were performed at an outside hospital and could not be obtained. In addition, we have no pathologic confirmation in 12 of 29 benign cases. Nonetheless, these cases showed no evidence of ma-

lignancy in physical examination, mammography, MRI, or sonography during the two-year follow-up, which suggests the benign nature of the lesions. Finally, this work presents potential selection bias, given that we included more cases with calcification than ones without calcification. A prospective study enrolling a larger cohort should be conducted to verify the results presented in this work.

In conclusion, the combination of DCE-MRI and ADC values is valuable for improving the specificity for disease manifesting as primary AD detected by mammography. Breast MRI can be a useful tool when an equivocal finding of AD is presented on conventional mammography.

Conflict of interest disclosure

The authors declared no conflicts of interest.

References

1. American College of Radiology. Illustrated breast imaging reporting and data system (BI-RADS): ultrasound. Reston, VA: American College of Radiology, 2003.
2. Knutzen AM, Gisvold JJ. Likelihood of malignant disease for various categories of mammographically detected, nonpalpable breast lesions. Mayo Clin Proc 1993; 68:454–460. [CrossRef]
3. Shaheen R, Schimmelpenninck CA, Stoddart L, Raymond H, Slanetz PJ. Spectrum of diseases presenting as architectural distortion on mammography: multimodality radiologic imaging with pathologic correlation. Semin Ultrasound CT MR 2011; 32:351–362. [CrossRef]
4. Rangayyan RM, Banik S, Desautels JE. Computer-aided detection of architectural distortion in prior mammograms of interval cancer. J Digit Imaging 2010; 23:611-631.
5. Burrell HC, Sibbering DM, Wilson AR, et al. Screening interval breast cancers: mammographic features and prognosis factors. Radiology 1996; 199:811–817. [CrossRef]
6. Baker JA, Rosen EL, Lo JY, et al: Computer-aided detection (CAD) in screening mammography: Sensitivity of commercial CAD systems for detecting architectural distortion. AJR Am J Roentgenol 2003; 181:1083–1088. [CrossRef]
7. Boyer B, Russ E. Anatomical-radiological correlations: architectural distortions. Diagn Interv Imaging 2014; 95:134–140. [CrossRef]
8. Gennaro G, Toledano A, di Maggio C, et al. Digital breast tomosynthesis versus digital mammography: a clinical performance study. Eur Radiol 2010; 20:1545–1553. [CrossRef]
9. Michell MJ, Iqbal A, Wasan RK, et al. A comparison of the accuracy of film-screen mammography, full-field digital mammography, and digital breast tomosynthesis. Clin Radiol 2012; 67: 976–981. [CrossRef]
10. Skaane P, Gullien R, Bjorndal H, et al. Digital breast tomosynthesis (DBT): initial experience in a clinical setting. Acta Radiol 2012, 53:524–529. [CrossRef]
11. Luparia A1, Mariscotti G, Durando M, et al. Accuracy of tumour size assessment in the preoperative staging of breast cancer: comparison of digital mammography, tomosynthesis, ultrasound and MRI. Radiol Med 2013; 118:1119–1136. [CrossRef]
12. Kuhl C. The current status of breast MR imaging. Part I. Choice of technique, image interpretation, diagnostic accuracy, and transfer to clinical practice. Radiology 2007; 244:356–378. [CrossRef]
13. Kuhl CK. Current status of breast MR imaging. Part 2. Clinical applications. Radiology 2007; 244:672–691. [CrossRef]
14 Bluemke DA, Gatsonis CA, Chen MH, et al. Magnetic resonance imaging of the breast prior to biopsy. JAMA 2004; 292:2735–2742. [CrossRef]
15. Hrung JM, Sonnad SS, Schwartz JS, Langlotz CP. Accuracy of MR imaging in the work-up of suspicious breast lesions: a diagnostic meta-analysis. Acad Radiol 1999; 6:387–397. [CrossRef]
16. Peters NH, Borel Rinkes IH, Zuithoff NP, Mali WP, Moons KG, Peeters PH. Meta-analysis of MR imaging in the diagnosis of breast lesions. Radiology 2008; 246:116–124. [CrossRef]
17. Ei Khouli RH, Jacobs MA, Mezban SD, et al. Diffusion-weighted imaging improves the diagnostic accuracy of conventional 3.0-T breast MR imaging. Radiology 2010; 256:64–73. [CrossRef]
18. Tsushima Y, Takahashi-Taketomi A, Endo K. Magnetic resonance (MR) differential diagnosis of breast tumors using apparent diffusion coefficient (ADC) on 1.5-T. J Magn Reson Imaging 2009; 30:249–255. [CrossRef]
19. Partridge SC, Rahbar H, Murthy R, et al. Improved diagnostic accuracy of breast MRI through combined apparent diffusion coefficients and dynamic contrast-enhanced kinetics. Magn Reson Med 2011; 65:1759–1767. [CrossRef]
20. Kul S, Cansu A, Alhan E, Dinc H, Gunes G, Reis A. Contribution of diffusion-weighted imaging to dynamic contrast-enhanced MRI in the characterization of breast tumors. AJR Am J Roentgenol 2011; 196:210–217. [CrossRef]
21. Yabuuchi H, Matsuo Y, Okafuji T, et al. Enhanced mass on contrast-enhanced breast MR imaging: Lesion characterization using combination of dynamic contrast-enhanced and diffusion-weighted MR images. J Magn Reson Imaging 2008; 28:1157–1165. [CrossRef]
22. Yabuuchi H, Matsuo Y, Kamitani T, et al. Non-mass-like enhancement on contrast-enhanced breast MR imaging: lesion characterization using combination of dynamic contrast-enhanced and diffusion-weighted MR images. Eur J Radiol 2010; 75:e126–132. [CrossRef]
23. Buchberger W, DeKoekkoek-Doll P, Obrist P, Dunser M. Value of MR tomography in inconclusive mammography findings. Radiology 1997; 37:702–709.
24. Gilles R, Guinebretiere JM, Lucidarme O, et al. Nonpalpable breast tumors: diagnosis with contrast-enhanced subtraction dynamic MR imaging. Radiology 1994; 191:625–631. [CrossRef]
25. Schueller G, Riedl CC, Mallek R, et al. Image quality, lesion detection, and diagnostic efficacy in digital mammography: full-field digital mammography versus computed radiography-based mammography using digital storage phosphor plates. Eur J Radiol 2008; 67:487–496. [CrossRef]
26. Cilotti A, Iacconi C, Marini C, et al. Contrast-enhanced MR imaging in patients with BI-RADS 3-5 microcalcifications. Radiol Med 2007; 112:272–286. [CrossRef]
27. Uematsu T, Yuen S, Kasami M, Uchida Y. Dynamic contrast-enhanced MR imaging in screening detected microcalcification lesions of the breast: is there any value? Breast Cancer Res Treat 2007; 103:269–281. [CrossRef]
28. Guo Y, Cai YQ, Cai ZL, et al. Differentiation of clinically benign and malignant breast lesions using diffusion-weighted imaging. J Magn Reson Imaging 2002; 16:172–178. [CrossRef]
29. Yili Z, Xiaoyan H, Hongwen D, et al. The value of diffusion-weighted imaging in assessing the ADC changes of tissues adjacent to breast carcinoma. BMC Cancer 2009; 9:18. [CrossRef]
30. Stadlbauer A, Bernt R, Gruber S, et al. Diffusion-weighted MR imaging with background body signal suppression (DWIBS) for the diagnosis of malignant and benign breast lesions. Eur Radiol 2009; 19:2349–2356. [CrossRef]
31. Lo GG, Ai V, Chan JK, et al. Diffusion-weighted magnetic resonance imaging of breast lesions: first experiences at 3 T. J Comput Assist Tomogr 2009; 33:63–69. [CrossRef]
32. Partridge SC, Demartini WB, Kurland BF, Eby PR, White SW, Lehman CD. Differential diagnosis of mammographically and clinically occult breast lesions on diffusion-weighted MRI. J Magn Reson Imaging 2010; 31:562–570. [CrossRef]
33. Baltzer PA, Benndorf M, Dietzel M, Gajda M, Runnebaum IB, Kaiser WA. False-positive findings at contrast-enhanced breast MRI: a BI-RADS descriptor study. AJR Am J Roentgenol 2010; 194:1658–1663. [CrossRef]
34. Pereira FP, Martins G, Figueiredo E, et al. Assessment of breast lesions with diffusion-weighted MRI: comparing the use of different b values. AJR Am J Roentgenol 2009; 193:1030–1035. [CrossRef]
35. Partridge SC, Mullins CD, Kurland BF, et al. Apparent diffusion coefficient values for discriminating benign and malignant breast MRI lesions: effects of lesion type and size. AJR Am J Roentgenol 2010; 194:1664–1673. [CrossRef]
36. Tozaki M, Fukuda K. High-spatial-resolution MRI of non-masslike breast lesions: interpretation model based on BI-RADS MRI descriptors. AJR Am J Roentgenol 2006; 187:330–337. [CrossRef]
37. Kim SH, Cha ES, Kim HS, et al. Diffusion-weighted imaging of breast cancer: correlation of the apparent diffusion coefficient value with prognostic factors. J Magn Reson Imaging 2009; 30:615–620. [CrossRef]
38. Marini C, Iacconi C, Giannelli M, Cilotti A, Moretti M, Bartolozzi C. Quantitative diffusion-weighted MR imaging in the differential diagnosis of breast lesion. Eur Radiol 2007; 17:2646–2655. [CrossRef]
39. Liberman L, Mason G, Morris FA, et al. Does size matter? Positive predictive value of MRI-detected breast lesions as a function of lesion size. AJR Am J Roentgenol 2006; 186:426–430. [CrossRef]
40. Barreau B, de Mascarel I, Feuga C, et al. Mammography of ductal carcinoma in situ of the breast: review of 909 cases with radiographic-pathologic correlations. Eur J Radiol 2005; 54:55–61. [CrossRef]

41. Stomper PC, Connolly JL, Meyer JE, Harris JR. Clinically occult ductal carcinoma in situ detected with mammography: analysis of 100 cases with radiologic-pathologic correlation. Radiology 1989; 172:235–241. [CrossRef]

42. Jansen SA, Newstead GM, Abe H, Shimauchi A, Schmidt RA, Karczmar GS. Pure ductal carcinoma in situ: kinetic and morphologic MR characteristics compared with mammographic appearance and nuclear grade. Radiology 2007; 245:684–691. [CrossRef]

43. Rosen EL, Smith-Foley SA, DeMartini WB, Eby PR, Peacock S, Lehman CD. BI-RADS MRI enhancement characteristics of ductal carcinoma in situ. Breast J 2007; 13:545–550. [CrossRef]